The structural, mechanical, electronic, and optical properties of Janus Hf$_2$CXY (X, Y = O, S, Se or Te, X ≠ Y) MXenes

R. Huang, Y. Z. Wang*, C. B. Li, C. Dang
Faculty of Mathematics and Physics, Huaiyin Institute of Technology, Jiangsu, 223003, China

Janus functionalized MXenes have attracted growing interest due to their exceptional properties. In this work, the structural, mechanical, electronic, and optical properties of Janus Hf$_2$CXY (X, Y = O, S, Se or Te, X ≠ Y) MXenes are investigated using density functional theory. The results of the formation energy, phonon spectrum analysis, and elastic properties validate their structural stability. The Young's modulus (Y), shear modulus (G), and Poisson's ratio (v) of Janus Hf$_2$CXY MXenes can be modulated by the different surface functional groups. It is found that the Janus Hf$_2$COS is a semiconductor with an indirect band gap, while other Hf$_2$CXY MXenes exhibit metallic character. Furthermore, we also explore the effect of strain on the electronic and optical properties of Hf$_2$COS. The results show that the semiconductor to metal transition can occur under compressive strain, and the dielectric spectrum and static dielectric constant can be altered by the tensile strain. These results demonstrate Janus Hf$_2$CXY MXenes' potential applications in electronic and optical nanodevices.

1. Introduction

After the successful synthesis of the Janus MoSSe monolayer[1, 2], the two-dimensional (2D) Janus materials have attracted increasing research interest owing to their unique physical and chemical properties. The Janus 2D structure is a sandwich structure with different surface atoms, and the asymmetric surface atoms break the out-of-plane mirror symmetry of the 2D material, which can induce an intrinsic built-in electric field perpendicular to the in-plane, thereby the 2D materials have many exotic and superior properties. Hu et al. have found the Rashba spin splitting in Janus MXY (M = Mo, W, and X, Y = S, Se, Te) monolayers due to their intrinsic internal electric field[3]. The Janus MoSSe and WSeTe monolayers can be potential solar water-splitting photocatalysts with low electron-hole recombination rates due to the built-in electric field[4, 5]. Jin et al. have found that the MoSSe monolayer can be an ideal material for nanoscale sensors due to the presence of out-of-plane polarization[6]. Large piezoelectricity was found in Janus transition metal dichalcogenide (TMD) monolayer and multilayer[7-10]. Tunable valley polarization in MoSSe monolayer can be achieved by magnetic doping and strain engineering[11]. Recently,

---

similar to the Janus TMD dichalcogenide monolayer, many other Janus materials have been studied, such as Janus TMD halogenides[12, 13], Janus group-III chalcogenides[14-17], Janus group-IV chalcogenides[18, 19], and Janus MXenes[20-22].

MXenes are a new group of 2D layer transition metal carbides, nitrides, and carbonitrides, with the general formula $M_{n+1}X_nT_x$ (n=1, 2, or 3), where M is an early transition metal, X is C and/or N, and T represents surface functional groups (O, OH, F, and so on). Owing to their rich surface functional groups, MXenes exhibit many intriguing physicochemical properties, and various potential applications have received more attention, such as energy storage[23-26], sensors and biosensors[27-30], catalysis[31-34], optoelectronics[35-37], field-effect transistor[38]. Recently, Janus MXenes have drawn more and more attention due to their exotic physical and chemical properties. Fu et al. discovered that the Janus Mn_2CXX' (X, X′ = F, Cl, Br, I) monolayers have a high spin polarization and that the magnetic anisotropy can be modulated by replacing the adsorbed atoms and biaxial strains[39]. Zhang et al. found Janus Sc_2COT' (T′ = H, OH, F, Cl) MXenes are ferrimagnetic half-metals, and that Sc_2COHCl, Sc_2HCl, and Sc_2CFCl are suitable photocatalysts for water splitting[40]. In our previous article, we studied the tunable electronic, elastic, and optical properties of Janus Zr_2COT (T = S, Se, and Te) MXenes[41]. To the best of our knowledge, the research on the structural, electronic, mechanical, and optical properties of Janus Hf_2C-based MXenes is limited.

In this work, we systematically investigate the structural, mechanical, electronic, and optical properties of Janus Hf_2CXY (X, Y = O, S, Se or Te, X ≠ Y) MXenes by the density functional theory. The results demonstrate that six Janus MXenes are stable structures. The mechanical and electronic properties of Janus Hf_2CXY can be modulated by altering surface functional groups. Moreover, the electronic and optical properties of the Hf_2COS can be adjusted by strains.

2. Computational methods

Density functional theory (DFT) simulations were performed by using the Vienna ab initio simulation package (VASP)[42]. The projector augmented wave (PAW) pseudopotential method was used to treat the interaction between electron and ion[43]. The generalized gradient approximation (GGA) with Perdew-Burke-Ernzerhof (PBE) formalism was adopted to describe the exchange-correlation functional[44]. The cutoff energy of the plane wave basis was set to 500 eV. The Hellmann-Feynman force and energy convergence values were chosen 10^{-2} eV/Å and 10^{-5} eV, respectively. Monkhorst-Pack k-point grids of 15×15×1 and 21×21×1 were adopted for geometry optimization and electronic structure calculation, respectively[45]. A vacuum region of 20 Å along the z direction was adopted to avoid the interactions between adjacent images. To take into account the van der Waals (vdW) interaction, Grimme's dispersion correction method was used[46]. The Heyd-Scuseria-Ernzerhof (HSE06) hybrid functional method was used to calculate the electronic structures and optical properties[47]. The phonon spectra calculated using the density-functional perturbation theory (DFPT) method were used to check the dynamical stability[48]. Bader charge analysis was used to investigate the charge transfer between atoms[49].

3. Results and discussion

3.1. Structural and mechanical properties

Firstly, we optimized the Hf_2C monolayer built from the MAX phase Hf_2AlC by removing the Al atoms. The optimized lattice constant (*a*) of Hf_2C is 3.21 Å, which is consistent with the previous research[50]. Then, according to the structural symmetry of Janus Hf_2CXY (X, Y = O, S, Se or Te, X ≠ Y) MXene, we constructed four possible structural configurations for the surface functionalized atoms on the Hf_2C, as depicted in Fig. 1.
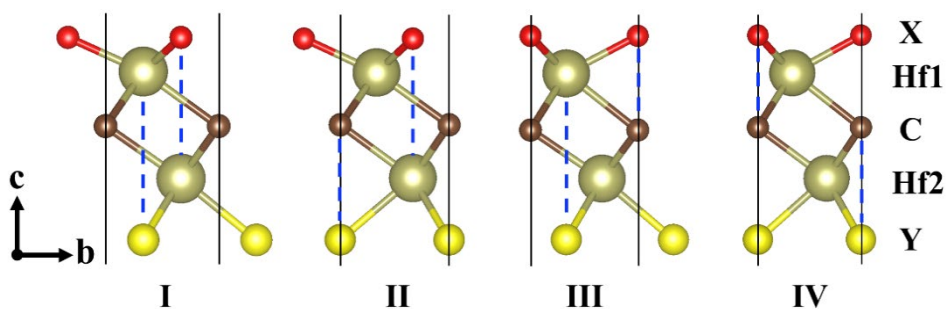

Fig. 1. Side views of different structural configurations for Janus Hf_2CXY MXenes.

For configuration I and II, X atoms are located above Hf2 atoms, and Y atoms reside below the Hf1 and C atoms, respectively. For configuration III and IV, X atoms locate at above C atoms, while Y atoms are positioned below the Hf1 and C atoms, respectively. Table 1 shows the relative energy of the four configurations for the Janus Hf_2CXY. We can see that the energy of configuration I is the lowest, implying the configuration I is energetically more favorable. To evaluate the stability of the Janus Hf_2CXY for configuration I, the formation energy (E_{form}) was calculated as follows[51]:

$$E_{form} = \frac{1}{5}\left(E_{Hf_2CXY} - E_{Hf_2C} - E_X - E_Y\right) \tag{1}$$

where E_{Hf_2CXY} and E_{Hf_2C} are the total energies of Hf_2CXY and Hf_2C, respectively. E_X (E_Y) is the energy per atom of the O_2 molecule, S_8 molecule, Se_8 molecule, or bulk Te. The calculated formation energies of the Hf_2CXY MXenes are all negative, as shown in Table 2, which means that the formation processes of Hf_2CXY MXenes are exothermic reactions, and all the systems are stable structures. In addition, the formation energies of Hf_2CXY MXenes gradually decrease with the decrease of electronegativity for surface functional atoms, which is in the order: Hf_2COS > Hf_2COSe > Hf_2COTe > Hf_2CSSe > Hf_2CSTe > Hf_2CSeTe. Table 2 displays the computed lattice constant, bond length, thickness, and charge transfer of Janus Hf_2CXY. It has been discovered that the bond lengths of Hf-O, Hf-S, Hf-Se, and Hf-Te increase gradually with the decrease of electronegativity from O to Te, while the lengths of the same chemical bonds are almost

unchanged in different systems. The lattice constant and the thickness of Janus Hf$_2$CXY increase with the order: Hf$_2$COS < Hf$_2$COSe < Hf$_2$COTe < Hf$_2$CSSe < Hf$_2$CSTe < Hf$_2$CSeTe, which is related with the bond length variation. As shown in Table 2, there are notable electron transfers from Hf atoms to surface atoms, indicating the strong ionic interaction between the Hf atoms and surface functional atoms. At the same time, the amounts of electron obtained of surface functional atoms are related to their electronegativity, and the total electron transferred from Hf atoms to surface functional atoms gradually decrease from Hf$_2$COS to Hf$_2$CSeTe, which is consistent with the variation of formation energy.

Table 1. Relative energy per unit cell for different configurations in eV of Janus Hf$_2$CXY MXenes.

Configuration	Hf$_2$COS	Hf$_2$COSe	Hf$_2$COTe	Hf$_2$CSSe	Hf$_2$CSTe	Hf$_2$CSeTe
I	0.00	0.00	0.00	0.00	0.00	0.00
II	0.50	0.47	0.29	0.54	0.39	0.41
III	1.02	0.92	0.74	0.53	0.43	0.38
IV	1.70	1.44	1.03	1.18	0.84	0.82

Table 2. The lattice constant (a), formation energy (E$_{form}$), bond length (l$_{Hf-X(Y)}$), thickness (h), and charge transfer (ΔQ) from Hf atoms to X and Y atoms for Janus Hf$_2$CXY MXenes.

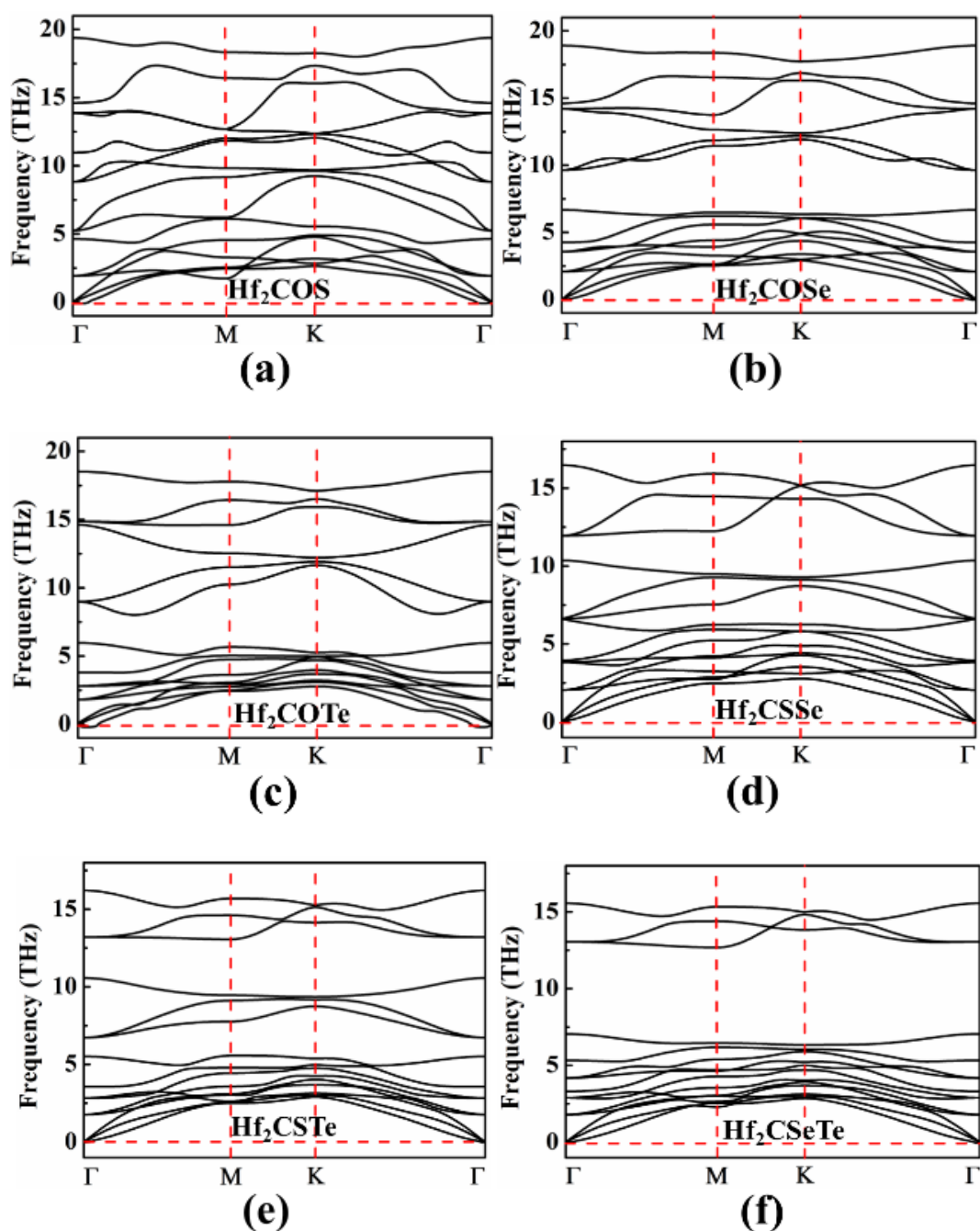| Type	a (Å)	E_{form} (eV/atom)	l_{Hf-X} (Å)	l_{Hf-Y} (Å)	h (Å)	ΔQ_X (e)	ΔQ_Y (e)
Hf$_2$COS	3.36	-2.01	2.13	2.49	5.16	1.43	0.50
Hf$_2$COSe	3.37	-1.94	2.13	2.64	5.34	1.27	0.34
Hf$_2$COTe	3.38	-1.75	2.14	2.88	5.63	1.44	0.17
Hf$_2$CSSe	3.47	-1.36	2.51	2.65	5.88	0.69	0.45
Hf$_2$CSTe	3.48	-1.19	2.51	2.91	6.15	0.77	0.17
Hf$_2$CSeTe	3.51	-1.14	2.63	2.90	6.28	0.55	0.10

Fig. 2. Phonon dispersion spectra of Janus Hf₂CXY MXenes.

To evaluate Janus Hf$_2$CXY MXenes' dynamical stability, we calculated their phonon dispersion relations, as shown in Fig. 2. There are fifteen vibrational phonon modes in all the phonon spectra, including three low frequency optical phonon modes and twelve high frequency optical phonon modes. For the six Janus structures, there are no imaginary frequencies in the Brillouin zone, proving the dynamical stability of all the systems investigated. The maximum frequencies of the phonon spectra are 19.4-15.6 THz (640.2-514.8 cm^{-1}) from Hf$_2$COS to Hf$_2$CSeTe, which is higher than the highest frequency of MoS$_2$ (461.6 cm^{-1})[52], meaning the

chemical bonds of Hf atoms and surface functional atoms are rather strong.

Next, the mechanical stability and properties of Janus Hf_2CXY MXenes are investigated using the elastic constants C_{ij}. For the hexagonal symmetry of Janus Hf_2CXY, there are only two independent elastic constants C_{11} and C_{12}, and $C_{66} = (C_{11} - C_{12})/2$. The Young's modulus ($Y$), shear modulus ($G$), and Poisson's ratio ($v$) of Janus Hf_2CXY can be obtained by

$$Y = \frac{C_{11}^2 - C_{12}^2}{C_{11}} \tag{2}$$

$$G = C_{66} \tag{3}$$

$$\upsilon = \frac{C_{12}}{C_{11}} \tag{4}$$

Table 3 shows the calculated elastic constants, Young's modulus, shear modulus (G), and Poisson's ratio. It can be seen that all the elastic constants of Janus Hf_2CXY obey the Born criteria of mechanical stability: $C_{11}^2 - C_{12}^2 > 0$ and $C_{66} > 0$. From table 3, we find that the Young's modulus of Janus Hf_2COY (Y = S, Se, Te) decreases with the increase of bond length l_{Hf-Y}, which is similar to the variation trend of Zr_2COT (T= S, Se, Te)[41]. And the Young's modulus of Hf_2COTe, Hf_2CSTe, and Hf_2CSeTe are 119.36, 129.01, and 127.93 Nm^{-1}, respectively, which are almost the same and they are smaller than 178.16 Nm^{-1} for Hf_2COS, 175.11 Nm^{-1} for Hf_2COSe, and 160.17 Nm^{-1} for Hf_2CSSe. We also find the shear modulus has the same variation trend as the Young's modulus for Hf_2CXY, as shown in Table 3. Moreover, the Poisso's ratios of Hf_2COTe, Hf_2CSTe, and Hf_2CSTe are also almost the same, which are larger than those of Hf_2COS, Hf_2COSe, and Hf_2CSSe. These results may be because the chemical bond of Hf-Te is weaker than that of Hf-O, Hf-S, and Hf-Se, while the weakest chemical bond has an important effect on the mechanical properties.

Table 3. The calculated elastic constant (C_{ij}), shear modulus (G), Young's modulus (Y), and Posson's ratio (v) of Janus Hf_2CXY MXenes.

Type	$C_{11}=C_{22}$ (Nm^{-1})	C_{12} (Nm^{-1})	$G=C_{66}$ (Nm^{-1})	Y (Nm^{-1})	v
Hf_2COS	197.92	62.53	67.70	178.16	0.32
Hf_2COSe	192.17	57.25	67.46	175.11	0.30
Hf_2COTe	158.40	78.64	39.88	119.36	0.50
Hf_2CSSe	177.19	54.92	61.14	160.17	0.31
Hf_2CSTe	161.08	71.87	44.61	129.01	0.45
Hf_2CSeTe	161.54	73.68	43.93	127.93	0.46

3.2. Electronic properties

After carefully examining the structural stability, we calculated the energy band structures of Janus Hf$_2$CXY MXenes, as shown in Fig. 3. According to Fig. 3(a), the Hf$_2$COS exhibits an indirect band gap band semiconductor with the valence band maximum (VBM) and the conduction band minimum (CBM) at the Γ and M point, respectively, and the band gap is 0.47 eV. Moreover, we find the Hf$_2$COSe, Hf$_2$COTe, Hf$_2$CSSe, Hf$_2$CSTe, and Hf$_2$CSeTe are all metallic, as shown in Fig. 3(b)-(f). Therefore, the semiconductor to metal transition can be realized by changing the surface functional groups for Hf$_2$C-based MXenes. To know more about the electronic characteristics of the Janus Hf$_2$CXY MXenes, we calculated their total and partial density of states (PDOS), as shown in Fig. 4. Fig. 4(a) illustrates that the VBM and CBM of Hf$_2$COS are contributed mainly by the S-p and Hf-d states, respectively. At the same time, as shown in Fig. 4(b)-(f), the Hf-d, Se-p, and Te-p orbitals cross the fermi level, which shows that the Hf$_2$COSe, Hf$_2$COTe, Hf$_2$CSSe, Hf$_2$CSTe, and Hf$_2$CSeTe are all metallic nature.
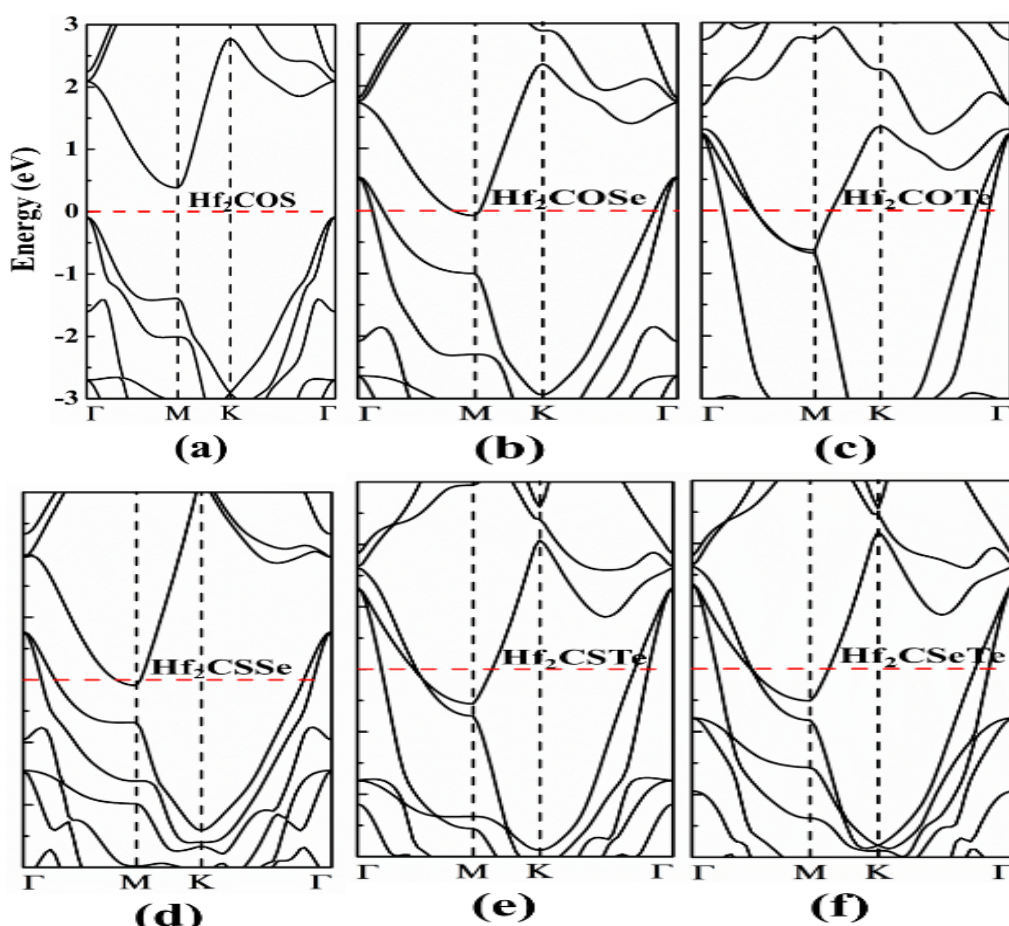

Fig. 3. Electronic band structures of Janus Hf$_2$CXY MXenes. The Fermi level is set at 0 eV.
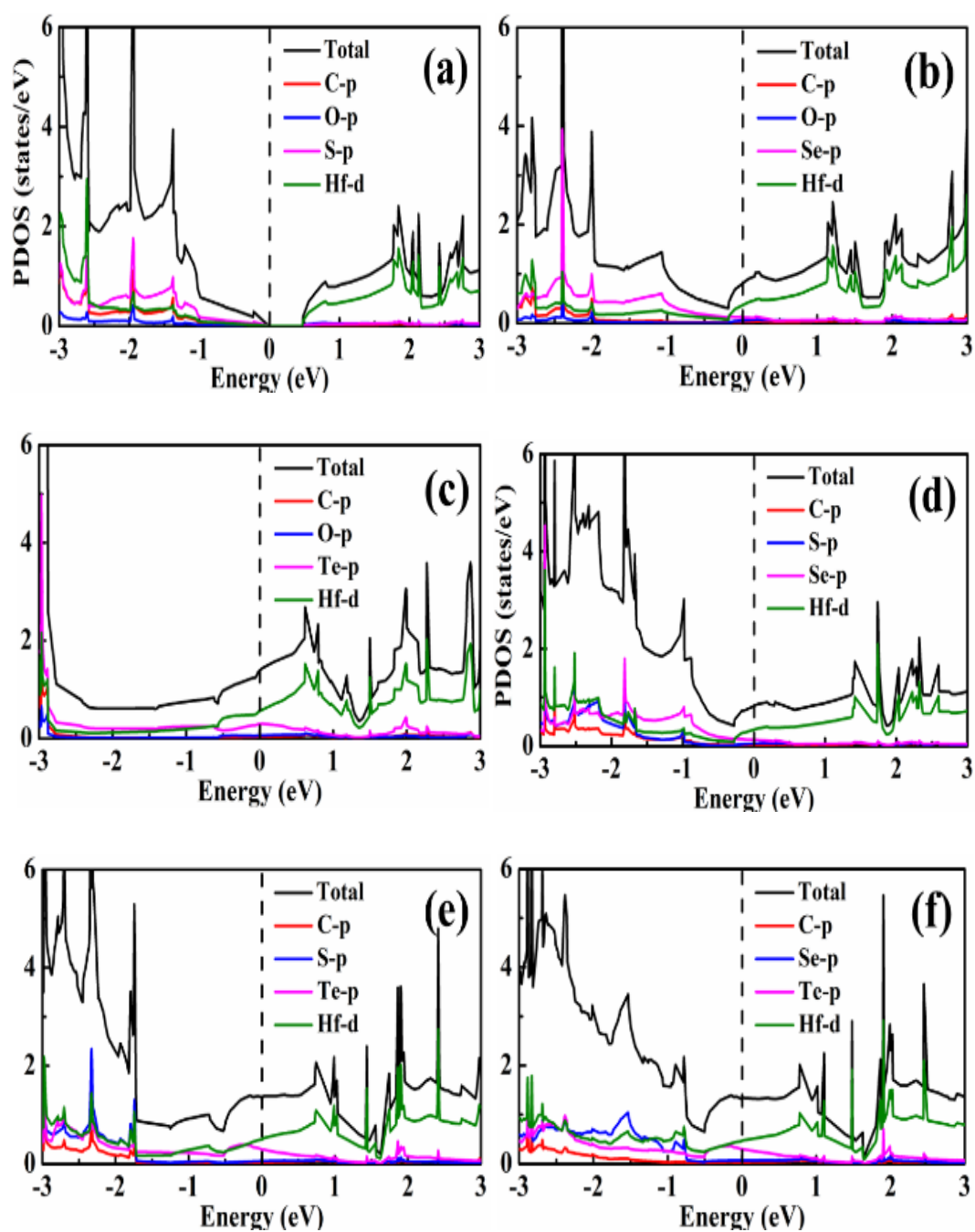
778

Fig. 4. The TDOS and PDOS of Janus (a) Hf₂COS, (b) Hf₂COSe, (c) Hf₂COTe, (d) Hf₂CSSe, (e) Hf₂CSTe, and (f) Hf₂CSeTe MXenes. The Fermi energy is set at 0 eV.
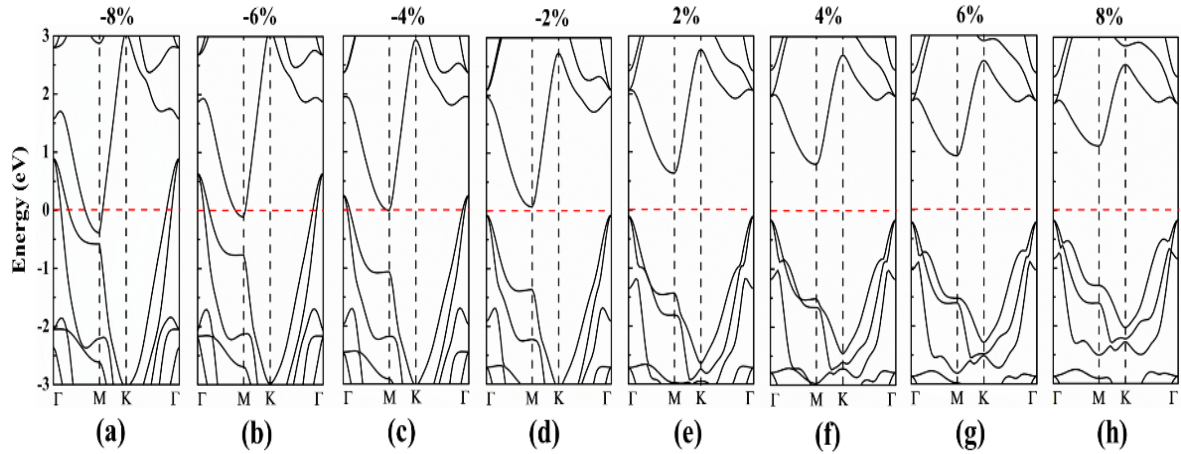
Fig. 5. Electronic band structures of Janus Hf$_2$COS MXene under biaxial strains. The Fermi level is set at 0 eV.

It is well known that strain is an effective method to modulate the electronic properties of 2D materials. Then we studied the influence of the biaxial strain on the electronic structures of the Janus Hf$_2$COS MXene. The strain is defined as $\varepsilon = (a - a_0)/a_0$, where a_0 and a are the lattice constants of unstrained and strained systems, respectively. The tensile and compressive strains are represented by positive and negative values, respectively. Fig. 5 illustrates the band structures of Hf$_2$COS under strains. It can be seen that the band gap of Hf$_2$COS increases gradually with the increase of the tensile strain, band gaps are 0.74, 0.96, 1.14 and 1.28 eV for strains of 2%, 4%, 6%, and 8%, respectively. While the band gap narrows under the compressive strain, especially, the Hf$_2$COS becomes metal when the compressive strain reaches 4%. Therefore, the semiconductor to metal transition can be realized by the suitable compressive strain.

3.3. Optical properties

As discussed above, the Janus Hf$_2$COS has a suitable band gap under strain for the application of optoelectronic devices. So, it is interesting to investigate the effect of tensile strain on the optical properties of the Janus Hf$_2$COS. The optical properties can be studied by the complex dielectric function $\varepsilon(\omega) = \varepsilon_1(\omega) + i\varepsilon_2(\omega)$. The imaginary part $\varepsilon_2(\omega)$ of the dielectric function is given by the following formula[53]:

$$\varepsilon_2 = \frac{4\pi^2 e^2}{\Omega} \lim_{q \to 0} \frac{1}{q^2} \sum_{c,v,k} 2\omega_k \delta(\varepsilon_{ck} - \varepsilon_{vk} - \omega) \times \langle u_{ck} + e_{\alpha q} | u_{vk} \rangle \langle u_{ck} + e_{\beta q} | u_{vk} \rangle^* \tag{5}$$

where the indices c and v refer to conduction and valence band states, respectively. The real part $\varepsilon_1(\omega)$ can be obtained from $\varepsilon_2(\omega)$ using the Kramers-Kronig relation as:

$$\varepsilon_1(\omega) = 1 + \frac{2}{\pi} P \int_0^\infty \frac{\varepsilon_2^{\alpha\beta}(\omega')\omega'}{\omega'^2 - \omega^2 + i\eta} d\omega' \qquad (6)$$

where P stands for the principal value of the integral, and η is an infinitesimal number that denotes the complex shift. Fig. 6 shows the real and imaginary part of the dielectric function of Janus Hf_2COS Mxene under different tensile strains. Due to the structural anisotropy, the real and imaginary parts are considered along the in-plane and out-of-plane directions. From Fig. 6, we can see the real and imaginary parts exhibit strong anisotropy in two different directions, and they can be altered via the tensile strains. With increasing tensile strains, there are obvious blue shifts for the real and imaginary parts along the in-plane direction, in contrast, the peak positions along the out-of-plane direction of them appear red shifts. Moreover, the real and imaginary parts along the in-plane direction have obvious red shifts as compared to those along the out-of-plane direction. The static dielectric constants ($\varepsilon_1(0)$) of the Hf_2COS under tensile strain are shown in Fig. 7, and which can be seen that the static dielectric constants along the in-plane and out-of-plane directions decrease gradually with increasing tensile strains. From the imaginary part as shown in Fig. 6(c) and (d), we can see the light absorption of Hf_2COS is mainly located in the regions of visible light (1.6 ~ 3.1 eV). Moreover, the absorption peak along the in-plane direction exhibits an appropriate enhancement with increasing tensile strains, while the absorption peak along the out-of-plane direction presents the opposite trend. These results suggest that the Janus Hf_2COS could be a promising material for novel optoelectronic devices.
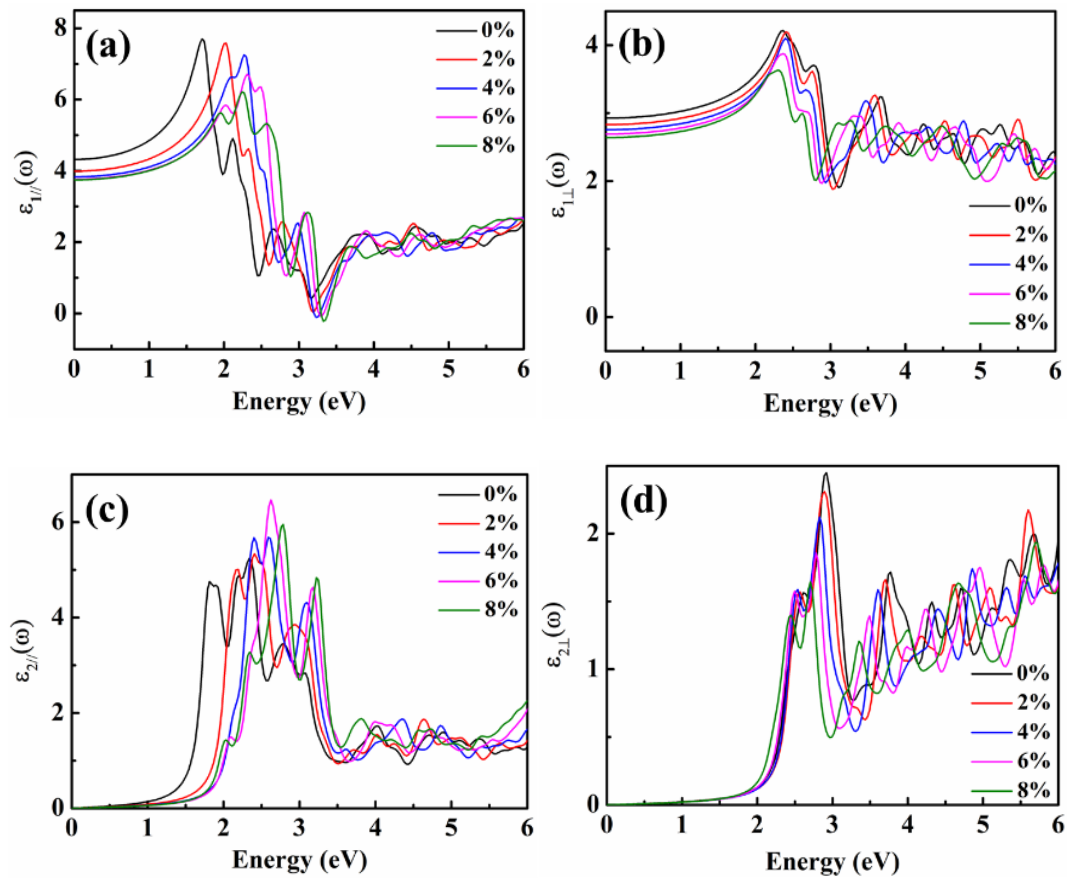

Fig. 6. Real part ε_1 and imaginary part ε_2 of the dielectric function for the Hf_2COS under tensile strain. The symbols of // and $\perp$ represent along the in-plane direction and out-of-plane direction, respectively.
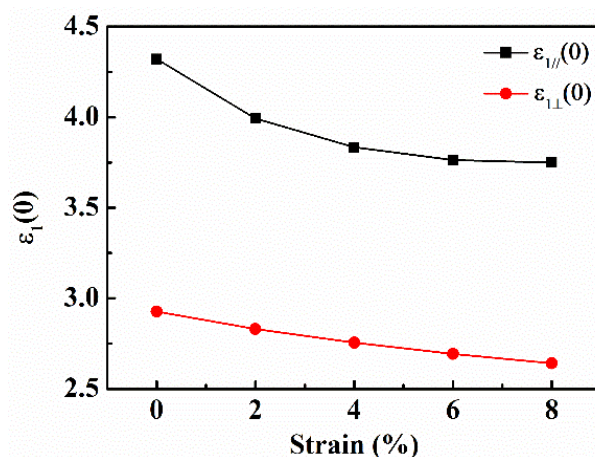
Fig. 7. Static dielectric constant $\varepsilon_1(0)$ of the Hf$_2$COS under tensile strain.

4. Conclusions

In this work, we studied the structural, mechanical, electronic, and optical properties of Janus Hf$_2$CXY (X, Y = O, S, Se or Te, X ≠ Y) MXenes by density functional theory. Their structural stability is verified by the formation energy, phonon spectrum analysis, and elastic characteristics. The Young's modulus (Y), shear modulus (G), and Poisson's ratio (v) of Janus Hf$_2$CXY MXenes can be altered by the different surface functional groups. It is found that the Hf$_2$COS is an indirect band gap semiconductor, while other Hf$_2$CXY MXenes exhibit metallic properties. Furthermore, the band gap of the Hf$_2$COS can be continuously tuned under strain. Especially, the semiconductor to metal transition can occur under suitable compressive strain. Under tensile strain, the dielectric spectra along the in-plane and out-of-plane directions occur blue shift and red shift, respectively, while the static dielectric constants in different directions decrease monotonically. Interestingly, the absorption peak along the in-plane direction exhibits an appropriate enhancement with increasing tensile strain. These results suggest the Janus Hf$_2$CXY MXenes can be a promising material for nanoelectronic and optoelectronic devices.

References

[1] A.Y. Lu, H.Y. Zhu, J. Xiao, C.P. Chuu, Y.M. Han, M.H. Chiu, C.C. Cheng, C.W. Yang, K.H. Wei, Y.M. Yang, Y. wang, D. Sokaras, D. Nordlund, P.D. Yang, D.A. Muller, M.Y. Chou, X. Zhang, L.J. Li, Nat. Nanotech. 12(8), 744 (2017); https://doi.org/10.1038/nnano.2017.100

[2] J. Zhang, S. Jia, I. Kholmanov, L. Dong, D.Q. Er, W.B. Chen, H. Guo, Z.H. Jin, V.B. Shenoy, L. Shi, J. Lou, ACS Nano 11(8), 8192 (2017); https://doi.org/10.1021/acsnano.7b03186

[3] T. Hu, F.H. Jia, G.D. Zhao, J.Y. Wu, A. Stroppa, W. Ren, Phys. Rev. B 97(23), 235404 (2018); https://doi.org/10.1103/PhysRevB.97.235404

[4] X.C. Ma, X. Wu, H.D. Wang, Y.C. Wang, J. Mater. Chem. A 6(5), 2295 (2018); https://doi.org/10.1039/C7TA10015A

[5] P. Jamdagni, R. Pandey, K. Tankeshwar, Nanotechnology 33(2), 025703 (2021); https://doi.org/10.1088/1361-6528/ac2d46

[6] J. Cui, X. Tang, X. Tan, S.C. Smith, Y. Dai, L.Z. Kou, J. Mater. Chem. A 7(3), 1099 (2019); https://doi.org/10.1039/C8TA08407F

[7] L. Dong, J. Lou, V.B. Shenoy, ACS Nano 11(8), 8242 (2017); https://doi.org/10.1021/acsnano.7b03313

[8] H.F. Cai, Y.F. Guo, H.J. Gao, W.L. Guo, Nano Energy 56, 33 (2019); https://doi.org/10.1016/j.nanoen.2018.11.027

[9] M.J. Varjovi, M. Yagmurcukardes, F.M. Peeters, E. Durgun, Phys. Rev. B 103(19), 195438 (2021); https://doi.org/10.1103/PhysRevB.103.195438

[10] M. Yagmurcukardes, F.M. Peeters, Phys. Rev. B 101(15), 155205 (2020); https://doi.org/10.1103/PhysRevB.101.155205

[11] R. Peng, Y.D. Ma, S. Zhang, B.B. Huang, Y. Dai, J. Phys. Chem. Lett. 9(13), 3612 (2018); https://doi.org/10.1021/acs.jpclett.8b01625

[12] F. Zhang, W.B. Mi, X.C. Wang, Adv. Electron. Mater. 6(1), 1900778 (2020); https://doi.org/10.1002/aelm.201900778

[13] M. Xiong, Z.Y. Chen, C.E. Hu, Y. Cheng, H.Y. Geng, Mater. Today Commun. 26, 101995 (2021); https://doi.org/10.1016/j.mtcomm.2020.101995

[15] A.J. Huang, W.W. Shi, Z.G. Wang, J. Phys. Chem. C 123(18), 11388 (2019); https://doi.org/10.1021/acs.jpcc.8b12450

[16] Y. Guo, S. Zhou, Y.Z. Bai, J.J. Zhao, Appl. Phys. Lett. 110(16), 163102 (2017); https://doi.org/10.1063/1.4981877

[17] T.V. Vu, T.P.T. Linh, H.V. Phuc, C.A. Duque, A.I. Kartamyshev, N.N. Hieu, J. Phys.: Condens. Matter 34(4), 045501 (2022); https://doi.org/10.1088/1361-648X/ac316e

[18] R. Gupta, B. Dongre, C. Bera, J. Carrete, J. Phys. Chem. C 124(32), 17476 (2020); https://doi.org/10.1021/acs.jpcc.0c03414

[19] T.V. Vu, H.V. Phuc, C.V. Nguyen, A.I. Kartamyshev, N.N. Hieu, J. Phys. D: Appl. Phys. 54(47), 475306 (2021); https://doi.org/10.1088/1361-6463/ac1d73

[20] W. Jin, S.Y. Wu, Z.G. Wang, Physica E 103, 307 (2018); https://doi.org/10.1016/j.physe.2018.06.024

[21] B. Akgenc, Comp. Mater. Sci. 171, 109231 (2020). https://doi.org/10.1016/j.commatsci.2019.109231

[22] S.L. Zhong, B. Xu, A. Cui, S.Y. Li, S.S. Liao, G.Q. Wang, G. Liu, B.Z. Sun, ACS Omega 5(1), 864 (2020); https://doi.org/10.1021/acsomega.9b03779

[23] W.X. Meng, X.J. Liu, H.Q. Song, Y. Xie, X.L. Shi, M. Dargusch, Z.G. Chen, Z.Y. Tang, S.Y. Lu, Nano Today 40, 101273 (2021); https://doi.org/10.1016/j.nantod.2021.101273

[24] H. Yu, Y.H. Wang, Y. Jing, J.M. Ma, C.F. Du, Q.Y. Yan, Small 15(25), 1901503 (2019); https://doi.org/10.1002/smll.201901503

[25] J. Yang, W.Z. Bao, P. Jaumaux, S.T. Zhang, C.Y. Wang, G.X. Wang, Adv. Mater. Interfaces 6(8), 1802004 (2019); https://doi.org/10.1002/admi.201802004

[26] F. Jamil, H.M. Ali, M.M. Janjua, J. Energy Storage 35, 102322 (2021); https://doi.org/10.1016/j.est.2021.102322

[27] S.K. Bhardwaj, H. Singh, M. Khatri, K.H. Kim, N. Bhardwaj, Biosens. Bioelectron. 202, 113995 (2022); https://doi.org/10.1016/j.bios.2022.113995

[28] S. Alwarappan, N. Nesakumar, D.L. Sun, T.Y. Hu, C.Z. Li, Biosens. Bioelectron. 205, 113943 (2022); https://doi.org/10.1016/j.bios.2021.113943

[29] R. Thenmozhi, S. Maruthasalamoorthy, R. Nirmala, R. Navamathavan, J. Electrochem. Soc. 168(11), 117507 (2021); https://doi.org/10.1149/1945-7111/ac2fc6

[30] K. Cheng, M.X. Wang, S.H. Wang, N.S. Liu, J.K. Xu, H. Wang, Y. Su, ACS Omega 7(11), 9267 (2022); https://doi.org/10.1021/acsomega.1c06027

[31] M.G. Ángel, C.V. Federico, I. Francesc, ACS Catal. 10(22), 13487 (2020); https://doi.org/10.1021/acscatal.0c03106

[32] N.G. Ma, Y.H. Wang, Y.Q. Zhang, B.C. Liang, J. Zhao, J. Fan, Appl. Surf. Sci. 596, 153574 (2022); https://doi.org/10.1016/j.apsusc.2022.153574

[33] X.W. Yang, Z.S. Lu, C. Cheng, Y. Wang, X.L. Zhang, Z.X. Yang, W.C. Lu, J. Phys. Chem. C 124(7), 4090 (2020); https://doi.org/10.1021/acs.jpcc.9b09912

[34] D.X. Kan, D.S. Wang, X.L. Zhang, R.Q. Lian, J. Xu, G. Chen, Y.J. Wei, J. Mater. Chem. A 8(6), 3097 (2020); https://doi.org/10.1039/C9TA12255A

[35] A. Mostafaei, M. Abbasnejad, J. Alloys Compd. 857, 157982 (2021); https://doi.org/10.1016/j.jallcom.2020.157982

[36] X.H. Li, L. Shan Shan, H.L. Cui, R.Z. Zhang, ACS Omega 5(35), 22248 (2020); https://doi.org/10.1021/acsomega.0c02435

[37] X.T. Jiang, A.V. Kuklin, A. Baev, Y.Q. Ge, H. Ågren, H. Zhang, P.N. Prasad, Phys. Rep. 848, 1 (2020); https://doi.org/10.1088/0034-4885/79/1/016501

[38] Ü.Ö. Akkuş, E. Balcı, S. Berber, Superlattices Microstruct. 140, 106433 (2020); https://doi.org/10.1016/j.spmi.2020.106433

[39] L.Q. Fu, X. Liu, B.Z. Zhou, X.C. Wang, Physica E 134, 114932 (2021); https://doi.org/10.1016/j.physe.2021.114932

[40] Y.G. Zhang, B.S. Sa, N.H. Miao, J. Zhou, Z.M. Sun, J. Mater. Chem. A 9(17), 10882 (2021); https://doi.org/10.1039/D1TA00614B

[41] Y.Z. Wang, Y. Tao, Q.F. Zhang, R. Huang, B.L. Gao, Z. Li, G.N. Li, N. Hu, Solid State Commun. 354, 114893 (2022); https://doi.org/10.1016/j.ssc.2022.114893

[42] G. Kresse, J. Furthmüller, Phys. Rev. B 54(16), 11169 (1996); https://doi.org/10.1103/PhysRevB.54.11169

[43] P.E. Blöchl, Phys. Rev. B 50(24), 17953 (1994); https://doi.org/10.1103/PhysRevB.50.17953

[44] J.P. Perdew, K. Burke, M. Ernzerhof, Phys. Rev. Lett. 77(18), 3865 (1996); https://doi.org/10.1103/PhysRevLett.77.3865

[45] H.J. Monkhorst, J.D. Pack, Phys. Rev. B 13(12), 5188 (1976); https://doi.org/10.1103/PhysRevB.13.5188

[46] S. Grimme, J. Comput. Chem. 27(15), 1787 (2006); https://doi.org/10.1002/jcc.20495

[47] J. Heyd, G.E. Scuseria, M. Ernzerhof, J. Chem. Phys. 118(18), 8207 (2003); https://doi.org/10.1063/1.1564060

[48] A. Togo, I. Tanaka, Scr. Mater. 108, 1 (2015); https://doi.org/10.1016/j.scriptamat.2015.07.021

[49] G. Henkelman, A. Arnaldsson, H. Jónsson, Comp. Mater. Sci. 36(3), 354 (2006); https://doi.org/10.1016/j.commatsci.2005.04.010

[50] H. Hadipour, Y. Yekta, Phys. Rev. B 100(19), 195118 (2019).

[51] S.E.M. Dilanga, J.J. Hu, J. Phys. Chem. C 125(23), 12469 (2021); https://doi.org/10.1021/acs.jpcc.1c00082

[52] B. Peng, H. Zhang, H. Shao, Y. Xu, X. Zhang, H. Zhu, RSC Adv. 6(7), 5767 (2016); https://doi.org/10.1039/C5RA19747C

[53] Y.Z. Wang, R. Huang, F.J. Kong, B.L. Gao, G.N. Li, F. Liang, G. Hu, Superlattices Microstruct. 132, 106156 (2019); https://doi.org/10.1016/j.spmi.2019.106156